Tensile Strain Effect on Thermoelectric Properties in Epitaxial $CaMnO_3$ Thin Films

Ebenezer Seesi , Mohammad El Loubani , Habib Rostaghi Chalaki , Avari Suber , Caden Kincaid , Dongkyu Lee *

Posted Date: 14 November 2025

doi: 10.20944/preprints202511.1059.v1

Keywords: oxide thermoelectrics; epitaxial thin films; oxygen vacancies; strain; carrier properties

Article

Tensile Strain Effect on Thermoelectric Properties in Epitaxial $CaMnO_3$ Thin Films

Ebenezer Seesi, Mohammed El Loubani, Habib Rostaghi Chalaki, Avari Suber, Caden Kincaid and Dongkyu Lee *

Department of Mechanical Engineering, University of South Carolina, Columbia, SC 29208, USA

* Correspondence: dongkyu@cec.sc.edu

Abstract

A deterministic platform for engineering epitaxial strain in $CaMnO_3$ (CMO) thermoelectric thin films is demonstrated using pulsed laser deposition, enabling precise control of the interplay between strain state and oxygen-vacancy formation. High-quality epitaxial CMO films are grown on four different single-crystalline substrates, which impose fully relaxed, partially relaxed, low-tensile, and high-tensile strain states, respectively. Increasing tensile strain induces a monotonic expansion of the unit-cell volume and a systematic rise in oxygen vacancy concentration. Oxygen vacancies increase carrier concentration but decrease mobility due to enhanced scattering. Reducing tensile strain suppresses vacancy scattering and increases both electrical conductivity (σ) and the Seebeck coefficient (S), mitigating the conventional inverse relationship between S and σ. Fully relaxed films exhibit σ approximately four orders of magnitude higher at room temperature than highly tensile-strained films. These relaxed films also show the highest power factor (PF = $S^2 \cdot \sigma$), exceeding strained films by up to six orders of magnitude. Strain-controlled oxygen vacancies thus provide a direct route to optimize charge transport and maximize the thermoelectric performance of CMO thin films.

Keywords: oxide thermoelectrics; epitaxial thin films; oxygen vacancies; strain; carrier properties

1. Introduction

Thermoelectric (TE) materials convert heat directly into electricity, offering a pathway for waste-heat recovery and decentralized power generation [1–3]. The TE conversion efficiency is quantified by the dimensionless figure of merit, $ZT = (\sigma S^2 T)/\kappa$, where σ, S, κ, and T are the electrical conductivity, Seebeck coefficient, thermal conductivity, and absolute temperature, respectively [4–6]. State-of-the-art performance has traditionally been achieved by heavy-metal chalcogenides, such as bismuth telluride (Bi_2Te_3) and lead telluride (PbTe) [7]. However, these compounds rely on scarce and toxic elements and often exhibit chemical and thermal instability at elevated temperatures, particularly in oxidizing environments [8,9]. Transition metal oxides are compelling alternatives due to their earth abundance, environmental benignity, and robust chemical/thermal stability under high-temperature, oxygen-rich conditions [10–12].

Among transition metal oxides, $CaMnO_{3-\delta}$ (CMO) has attracted increasing interest for n-type applications owing to its relatively large S and highly tunable electronic structure [9,13]. Despite these advantages, the overall TE efficiency of CMO remains modest due to its intrinsically low σ [9,14], which limits the power factor, PF = σS^2. While aliovalent cation substitution has been widely used to increase σ, optimizing the PF is challenging due to the strong interdependence between S and σ [15–18]. Increasing carrier concentration (n) typically reduces S, and vice versa, leading to a trade-off relationship [19–21].

In transition metal oxides, oxygen vacancies play a central role in this trade-off. As intrinsic point defects in ABO_3 systems, they increase n through $Mn^{4+} \rightarrow Mn^{3+}$ reduction, yet they also introduce scattering centers that degrade carrier mobility (μ) [22–24]. Thus, precise control of oxygen vacancy concentration is required for improving TE properties of oxides. Epitaxial strain has emerged as a

 doi:10.20944/preprints202511.1059.v1

powerful approach to tune oxygen vacancies, since strain can alter the concentration of oxygen vacancies [25–30]. Tensile strain, in particular, has been reported to lower the formation energy of oxygen vacancies, thereby increasing vacancy concentration and carrier density [23,31]. This strain–vacancy coupling offers a route to partially decouple S and σ, and thereby enhance PF.

Despite these insights, the explicit impact of strain-induced oxygen vacancies on the TE properties of CMO is not fully understood [32–35]. In this study, we investigate this effect by synthesizing high-quality epitaxial n-type CMO thin films via pulsed laser deposition (PLD). Epitaxial CMO films are deposited on single-crystalline $SrTiO_3$ (STO), $(LaAlO_3)_{0.3}(Sr_2TaAlO_6)_{0.7}$ (LSAT), $SrLaAlO_4$ (SLAO), and $LaAlO_3$ (LAO) substrates, which impose different strain states ranging from fully relaxed (STO) to tensile-strained (LAO). This platform enables direct correlation between strain state, oxygen-vacancy concentration, and charge-transport metrics, revealing a pathway to suppress vacancy scattering, mitigate the S-σ trade-off, and maximize PF for oxide TE devices.

2. Materials and Methods

2.1. Synthesis and Characterization of Thin Films.

Epitaxial CMO thin films with a film thickness of ~200 nm were grown on (001)-oriented substrates: SLAO (a = 3.756 Å), LAO (a = 3.79 Å), LSAT (a = 3.865 Å), and STO (a = 3.905 Å). These substrates impose different strain states on CMO (a = 3.72 Å); tensile strain (LAO, SLAO), partial relaxation (LSAT), and complete relaxation (STO) through lattice mismatch. Prior to deposition, substrates were mounted on the PLD substrate holder using silver paste (Leitsilber 200, Ted Pella, USA), heated for 15 min, and fixed into the chamber. High-quality CMO films were deposited using PLD with a KrF excimer laser (λ = 248 nm) at a repetition rate of 5 Hz and pulse energy of 4 J/cm^2, under an oxygen partial pressure (pO_2) of 25 mTorr at 700 °C. Following deposition, the films were cooled to room temperature at 10 °C/min under a pO_2 of 100 mTorr for ~1 h.

High-resolution X-ray diffraction (HRXRD) with a four-circle diffractometer was used to examine the crystallography and phase purity of all thin films at room temperature in both in-plane and out-of-plane configurations. Film thicknesses were confirmed by X-ray reflectivity (XRR). Strain states were analyzed by XRD reciprocal space mapping (RSM) around the substrates' 103 Bragg reflections.

2.2. Evaluation of TE and Carrier Properties

S was measured from 20 – 350 °C using a home-built measurement system based on the differential method of $S = \Delta V/\Delta T$, where ΔV is the electric potential induced by an applied temperature difference (ΔT) [36]. Two thermocouples were attached to the film ends using high-temperature resistant clips to ensure stable contacts. One end was heated, and both ΔV and ΔT were recorded and the resulting slope was taken as S.

σ was measured in the same temperature range using a van der Pauw electrode configuration with a DC voltage/current source/monitor (Keithley 2450 Sourcemeter). Both S and σ were first measured during heating (20 °C to 350 °C) and then repeated during cooling (350 °C to 20 °C) to confirm reproducibility. Carrier properties were further investigated through analysis of n and μ. Since Hall measurements are challenging for oxide thin films at elevated temperatures [37], the weighted mobility (μ_w) approach was employed. This method is well established and widely used in TE transport studies, providing reliable mobility trends when direct Hall data are impractical [37]. From μ_w, weighted carrier properties, including n_w, were extracted [38]. Calculation details are included in the Supporting Information.

 doi:10.20944/preprints202511.1059.v1

3. Results and Discussion

XRD θ-2θ scans at room temperature clearly show only 00*l* peaks from the CMO thin films, confirming (001)-oriented epitaxial growth on all substrates (Figure 1a). As shown in Figure 1b, the in-plane strain state varies with substrate: STO (fully relaxed, ε = 0.0%), LSAT (partially relaxed, ε = 0.39%), SLAO (low tensile strain, ε = ~ 0.47%), and LAO (high tensile strain, ε = ~ 0.84%). CMO films were coherently strained on LAO and SLAO, as indicated by the alignment of the film and substrate peaks along the in-plane (q_x) direction in RSM. By contrast, the large lattice mismatch on LSAT (~ 3.9%) and on STO (~ 4.79%) led to partial and complete relaxation, respectively. Accordingly, the CMO film peaks did not align with the LSAT and STO substrate peaks.

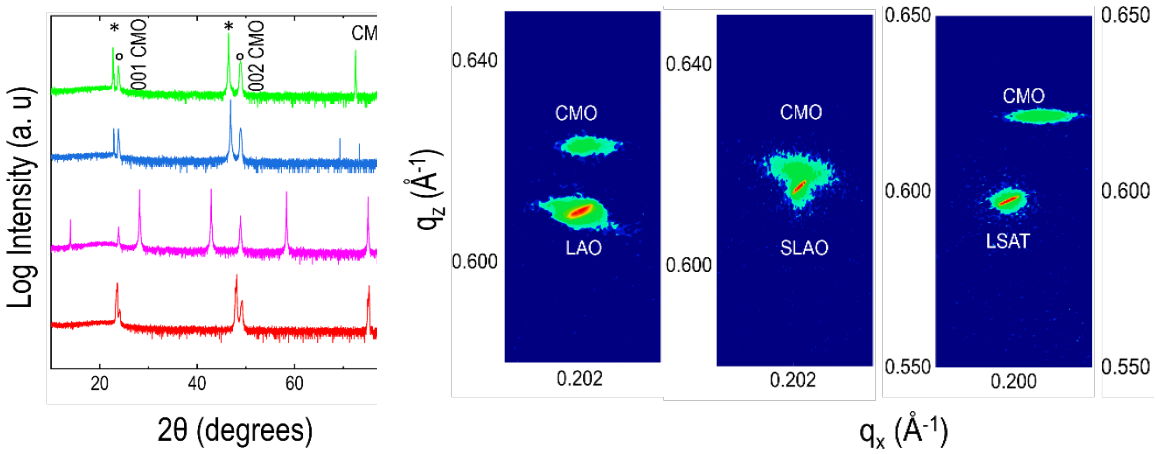

(**a**) (**b**)

Figure 1. (a) XRD θ-2θ patterns of the CMO thin films grown on LAO (red), SLAO (magenta), LSAT (blue), and STO (green) substrates (Substrate and film peaks are indicated with * and ° respectively); (b) XRD RSMs are shown around the asymmetric (103) reflection of the films and substrates.

To investigate how in-plane tensile strain affects oxygen vacancy concentration, we evaluated the unit cell volume of CMO from HRXRD since changes in δ in ABO_3 perovskites can modify the unit cell volume [25,27,39,40]. As shown in Figure 2, the unit-cell volume increased gradually from ~51.79 Å^3 (relaxed, STO) to ~52.32 Å^3 at ~0.84% tensile strain (LAO). This monotonic volume expansion is consistent with an increased oxygen vacancy concentration at larger tensile strain [22,26,31]. First-principles studies reported that tensile strain lowers the oxygen vacancy formation energy across perovskites, favoring vacancy formation and concomitant lattice expansion [23,41,42].

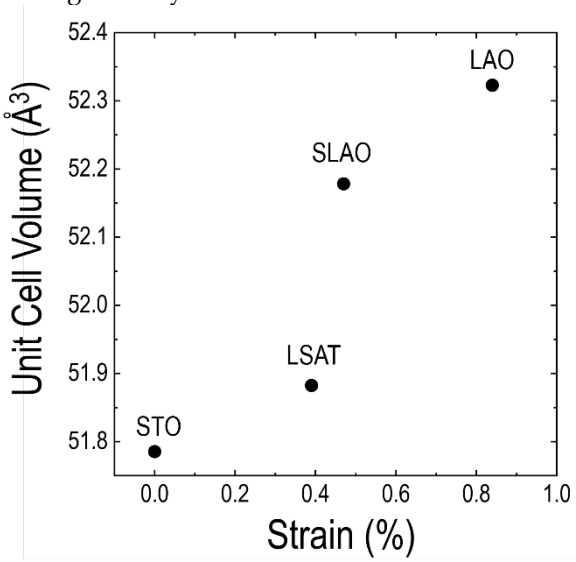

 doi:10.20944/preprints202511.1059.v1

Figure 2. Unit cell volume change as a function of strain state of the CMO thin films calculated from HRXRD measured at room temperature.

The temperature-dependent S and σ of the CMO thin films, measured from 0 °C to 350 °C are shown in Figure 3. For all samples, S remains negative over the entire range, confirming that CMO is an n-type semiconductor with electrons as the majority carriers (Figure 3a) [33,35]. The magnitude of S increases as the strain state decreases, from fully tensile strained CMO/LAO to fully relaxed CMO/STO. As shown in Figure 2, tensile strain promotes oxygen vacancy formation, which increases n [43] in CMO through $Mn^{4+} \rightarrow Mn^{3+}$ reduction [22,24]. Accordingly, reducing tensile strain lowers the degree of electron doping. For degenerate semiconductors, S is inversely proportional to n, with $S \propto n^{-2/3}$ [44,45]. Therefore, a decrease in n results in an increase in S, consistent with the trend observed in Figure 3a. At room temperature, the magnitude of S increases by nearly a factor of three when comparing the tensile-strained CMO/LAO with the fully relaxed CMO/STO. This observation agrees well with previous studies, showing that S decreases as n increases [45–48].

In contrast, σ decreased as tensile strain increased (Figure 3b). σ depends on both n and μ based on $\sigma = ne\mu$, with e the electrical charge of carrier [49,50]. While oxygen vacancies induced by tensile strain increase n, they also act as scattering centers that reduce μ [51], resulting in lower σ. Consequently, the unstrained CMO/STO film exhibits the highest σ, while the tensile-strained CMO/LAO shows the lowest. At room temperature, σ increases by nearly four orders of magnitude from the tensile-strained CMO/LAO to the fully relaxed CMO/STO.

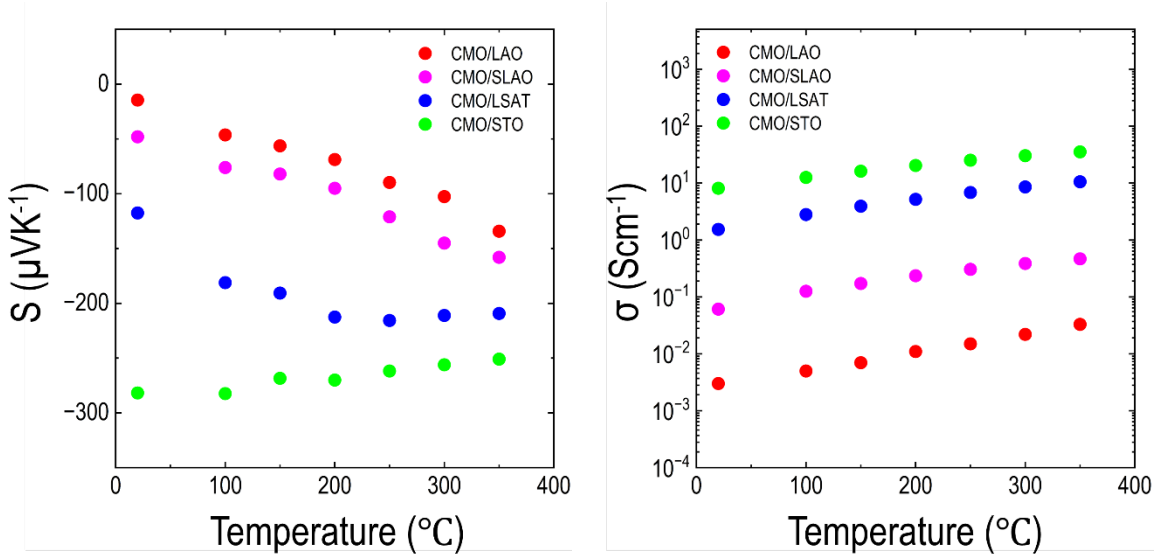

(**a**) (**b**)

Figure 3. Temperature dependencies of (a) S and (b) σ of the CMO thin films.

To study the influence of strain-induced oxygen vacancies on the carrier properties of the CMO thin films, we evaluated μ and n extracted from the measured S and σ over the entire temperature range (calculation details in the Supporting Information). Figure 4a shows the calculated weighted carrier concentration (n_w) as a function of temperature. n increased with increasing tensile strain, as expected, since tensile strain promotes oxygen vacancy formation and concomitant electron doping in CMO [43]. At room temperature, the tensile-strained CMO/LAO exhibited an n_w roughly one order of magnitude higher than that of the fully relaxed CMO/STO. This observation is consistent with the reduction in S with increasing tensile strain, shown in Figure 3a.

μ_w is a practical probe of charge transport, analogous to Hall mobility, and is widely used in TE studies owing to its robustness at elevated temperatures and suitability for low-mobility materials [37,52]. μ_w shows the opposite trend to n_w, decreasing with increasing tensile strain (Figure 4b). This

 doi:10.20944/preprints202511.1059.v1

behavior is attributed to strain-induced oxygen vacancies that act as scattering sites in the strained films [23]. As shown in Figure 4b, decreasing tensile strain increased μ_w by approximately six orders of magnitude for the unstrained CMO/STO at room temperature. This large μ_w enhancement outweighed the reduction in n and resulted in a substantial increase in σ for the unstrained film.

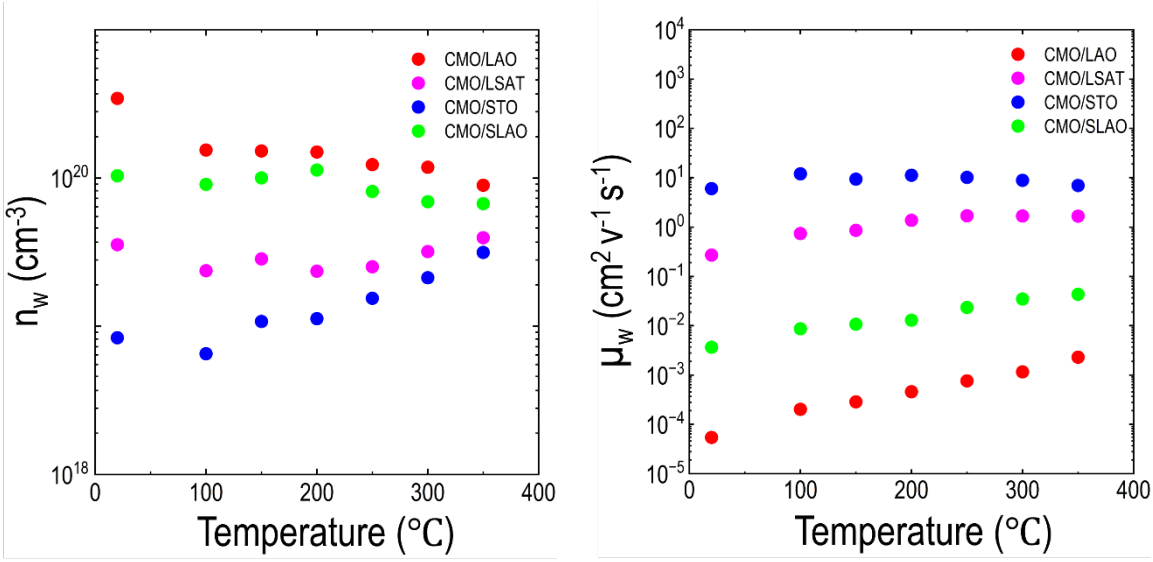

(**a**) (**b**)

Figure 4. Temperature dependence of (a) n_w and (b) μ_w for the CMO films.

We further evaluated the PF of the CMO thin films (Figure 5). PF increased with decreasing tensile strain over the entire temperature range (Figure 5a). At room temperature, the CMO/STO exhibited a PF more than six orders of magnitude higher than that of the tensile-strained CMO/LAO. This trend follows from the combination of higher σ and larger S in the unstrained films. A similar unusual trend has been reported for $La_{0.7}Ca_{0.2}Ni_{0.25}Ti_{0.75}O_{3-\delta}$, where PF increased by eight orders of magnitude owing to a synergistic rise in both S and σ [53]. These results indicate that modulating oxygen vacancies by tuning epitaxial strain can be an effective strategy to mitigate the conventional S-σ trade-off and improve TE performance.

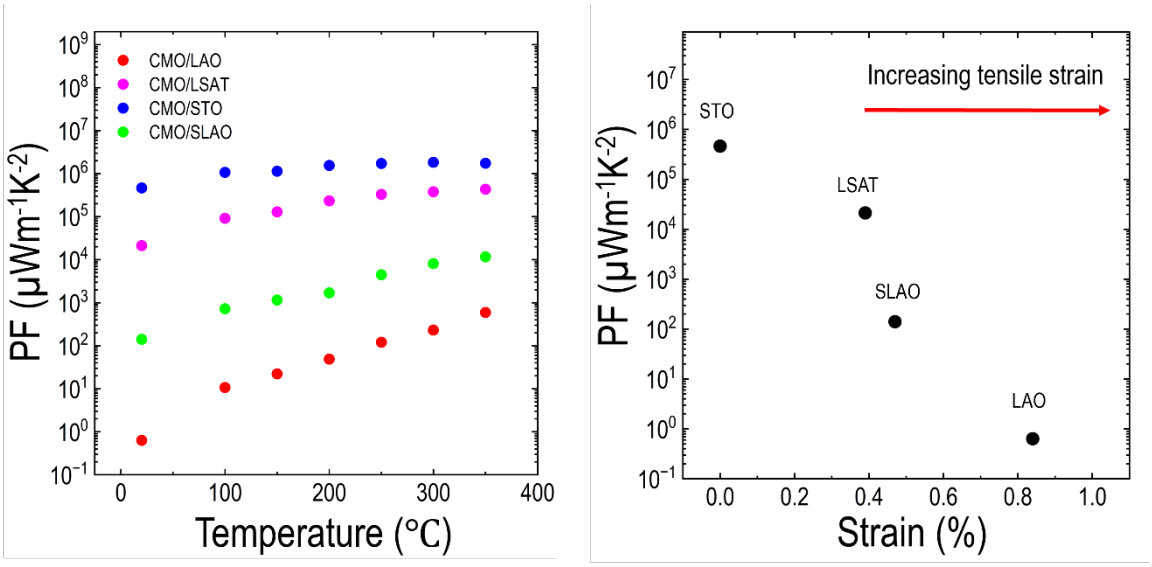

(**a**) (**b**)

 doi:10.20944/preprints202511.1059.v1

Figure 5. (a) Temperature dependence of PF of the CMO thin films. (b) PF as a function of strain state at room temperature.

5. Conclusions

In this study, we examined how strain-induced oxygen vacancies influenced the TE properties of CMO thin films. Lattice mismatch between CMO and the substrates was used to impose different epitaxial strain states. Epitaxial CMO films grown on LAO, SLAO, LSAT, and STO resulted in tensile-strained films on LAO and SLAO and partially or fully relaxed films on LSAT and STO, respectively. The TE properties improved as tensile strain decreased. This improvement is attributed to a reduction in strain-induced oxygen vacancies, which simultaneously led to increases in both σ and S. The combined enhancement of σ and S produced a substantial increase in PF, with an increase of approximately six orders of magnitude at room temperature. These findings demonstrate that modulation of oxygen vacancies through epitaxial strain is a promising strategy to improve the TE performance of oxide thin films and to mitigate the conventional S-σ trade-off.

Supplementary Materials: The Supporting Information is available free of charge at XX

Author Contributions: Conceptualization, D.L. and E.S.; formal analysis, E.S., M.E., H.R.; Investigation, E.S.; data curation, E.S., A.S., C. K.; writing—original draft preparation, E.S.; writing—review and editing, D.L., H.R.C.; supervision and project administration, D.L. All authors have read and agreed to the published version of the manuscript.

Funding: This research was funded by the National Science Foundation under NSF Award Number DMR-2340234.

Data Availability Statement: Raw data are available upon request.

Acknowledgments: Sample synthesis and structural characterization were conducted as part of a user project at the Center for Nanophase Materials Sciences (CNMS), which is a U.S. Department of Energy, Office of Science User Facility at Oak Ridge National Laboratory.

Conflicts of Interest: The authors declare no competing financial interest.

References

1. DiSalvo, F.J. Thermoelectric cooling and power generation. science 1999, 285, 703-706.
2. Chen, G.; Dresselhaus, M.; Dresselhaus, G.; Fleurial, J.-P.; Caillat, T. Recent developments in thermoelectric materials. International materials reviews 2003, 48, 45-66.
3. Snyder, G.J.; Toberer, E.S. Complex thermoelectric materials. Nature materials 2008, 7, 105-114.
4. Perumal, S.; Roychowdhury, S.; Biswas, K. Reduction of thermal conductivity through nanostructuring enhances the thermoelectric figure of merit in Ge 1− x Bi x Te. Inorganic Chemistry Frontiers 2016, 3, 125-132.
5. Alam, H.; Ramakrishna, S. A review on the enhancement of figure of merit from bulk to nano-thermoelectric materials. Nano energy 2013, 2, 190-212.
6. Channegowda, M.; Mulla, R.; Nagaraj, Y.; Lokesh, S.; Nayak, S.; Mudhulu, S.; Rastogi, C.K.; Dunnill, C.W.; Rajan, H.K.; Khosla, A. Comprehensive insights into synthesis, structural features, and thermoelectric properties of high-performance inorganic chalcogenide nanomaterials for conversion of waste heat to electricity. ACS Applied Energy Materials 2022, 5, 7913-7943.
7. Jabri, M.; Masoumi, S.; Sajadirad, F.; West, R.P.; Pakdel, A. Thermoelectric energy conversion in buildings. Materials Today Energy 2023, 32, 101257.
8. Liu, Y.; Zhi, J.; Li, W.; Yang, Q.; Zhang, L.; Zhang, Y. Oxide materials for thermoelectric conversion. Molecules 2023, 28, 5894.
9. Wang, Y.; Sui, Y.; Fan, H.; Wang, X.; Su, Y.; Su, W.; Liu, X. High temperature thermoelectric response of electron-doped CaMnO3. Chemistry of Materials 2009, 21, 4653-4660.

 doi:10.20944/preprints202511.1059.v1

10. Feng, Y.; Jiang, X.; Ghafari, E.; Kucukgok, B.; Zhang, C.; Ferguson, I.; Lu, N. Metal oxides for thermoelectric power generation and beyond. Advanced Composites and Hybrid Materials 2018, 1, 114-126.
11. Nag, A.; Shubha, V. Oxide thermoelectric materials: A structure–property relationship. Journal of electronic materials 2014, 43, 962-977.
12. Koumoto, K.; Terasaki, I.; Funahashi, R. Complex oxide materials for potential thermoelectric applications. MRS bulletin 2006, 31, 206-210.
13. Funahashi, R.; Kosuga, A.; Miyasou, N.; Takeuchi, E.; Urata, S.; Lee, K.; Ohta, H.; Koumoto, K. Thermoelectric properties of CaMnO 3 system. In Proceedings of the 2007 26th International Conference on Thermoelectrics, 2007; pp. 124-128.
14. Xu, S.; Wang, H.; Bu, T.a.; Wang, X.; Dong, Z.; Zhang, M.; Li, C.; Zhao, W. Utilization of doping and compositing strategy for enhancing the thermoelectric performance of CaMnO3 perovskite. Ceramics International 2024, 50, 37119-37125.
15. Van Du, N.; Rahman, J.U.; Huy, P.T.; Shin, W.H.; Seo, W.-S.; Kim, M.H.; Lee, S. X-site aliovalent substitution decoupled charge and phonon transports in XYZ half-Heusler thermoelectrics. Acta Materialia 2019, 166, 650-657.
16. Zhu, Y.; Wang, C.; Su, W.; Li, J.; Liu, J.; Du, Y.; Mei, L. High-temperature thermoelectric performance of Ca0. 96Dy0. 02RE0. 02MnO3 ceramics (RE= Ho, Er, Tm). Ceramics International 2014, 40, 15531-15536.
17. Zhu, Y.-H.; Su, W.-B.; Liu, J.; Zhou, Y.-C.; Li, J.; Zhang, X.; Du, Y.; Wang, C.-L. Effects of Dy and Yb co-doping on thermoelectric properties of CaMnO3 ceramics. Ceramics International 2015, 41, 1535-1539.
18. Thiel, P.; Eilertsen, J.; Populoh, S.; Saucke, G.; Döbeli, M.; Shkabko, A.; Sagarna, L.; Karvonen, L.; Weidenkaff, A. Influence of tungsten substitution and oxygen deficiency on the thermoelectric properties of CaMnO3− δ. Journal of Applied Physics 2013, 114.
19. Wang, J.; Yin, Y.; Che, C.; Cui, M. Research Progress of Thermoelectric Materials—A Review. Energies 2025, 18, 2122.
20. Dehkordi, A.M.; Zebarjadi, M.; He, J.; Tritt, T.M. Thermoelectric power factor: Enhancement mechanisms and strategies for higher performance thermoelectric materials. Materials Science and Engineering: R: Reports 2015, 97, 1-22.
21. Petsagkourakis, I.; Pavlopoulou, E.; Cloutet, E.; Chen, Y.F.; Liu, X.; Fahlman, M.; Berggren, M.; Crispin, X.; Dilhaire, S.; Fleury, G. Correlating the Seebeck coefficient of thermoelectric polymer thin films to their charge transport mechanism. Organic Electronics 2018, 52, 335-341.
22. Aschauer, U.; Pfenninger, R.; Selbach, S.M.; Grande, T.; Spaldin, N.A. Strain-controlled oxygen vacancy formation and ordering in CaMnO 3. Physical Review B—Condensed Matter and Materials Physics 2013, 88, 054111.
23. Mayeshiba, T.; Morgan, D. Strain effects on oxygen vacancy formation energy in perovskites. Solid State Ionics 2017, 311, 105-117.
24. Chandrasena, R.U.; Yang, W.; Lei, Q.; Delgado-Jaime, M.U.; Wijesekara, K.D.; Golalikhani, M.; Davidson, B.A.; Arenholz, E.; Kobayashi, K.; Kobata, M. Strain-engineered oxygen vacancies in CaMnO3 thin films. Nano letters 2017, 17, 794-799.
25. Yang, G.; El Loubani, M.; Chalaki, H.R.; Kim, J.; Keum, J.K.; Rouleau, C.M.; Lee, D. Tuning ionic conductivity in fluorite Gd-doped CeO2-Bixbyite RE2O3 (RE= Y and Sm) multilayer thin films by controlling interfacial strain. ACS Applied Electronic Materials 2023, 5, 4556-4563.
26. Yang, G.; El Loubani, M.; Handrick, D.; Stevenson, C.; Lee, D. Understanding the influence of strain-modified oxygen vacancies and surface chemistry on the oxygen reduction reaction of epitaxial La0. 8Sr0. 2CoO3-δ thin films. Solid State Ionics 2023, 393, 116171.
27. Lee, D.; Jacobs, R.; Jee, Y.; Seo, A.; Sohn, C.; Ievlev, A.V.; Ovchinnikova, O.S.; Huang, K.; Morgan, D.; Lee, H.N. Stretching epitaxial La0. 6Sr0. 4CoO3− δ for fast oxygen reduction. The Journal of Physical Chemistry C 2017, 121, 25651-25658.
28. Meyer, T.L.; Jacobs, R.; Lee, D.; Jiang, L.; Freeland, J.W.; Sohn, C.; Egami, T.; Morgan, D.; Lee, H.N. Strain control of oxygen kinetics in the Ruddlesden-Popper oxide La1. 85Sr0. 15CuO4. Nature communications 2018, 9, 92.

 doi:10.20944/preprints202511.1059.v1

29. Mayeshiba, T.; Morgan, D. Strain effects on oxygen migration in perovskites. Physical Chemistry Chemical Physics 2015, 17, 2715-2721.
30. Herklotz, A.; Lee, D.; Guo, E.-J.; Meyer, T.L.; Petrie, J.R.; Lee, H.N. Strain coupling of oxygen non-stoichiometry in perovskite thin films. Journal of Physics: Condensed Matter 2017, 29, 493001.
31. Aidhy, D.S.; Liu, B.; Zhang, Y.; Weber, W.J. Strain-induced phase and oxygen-vacancy stability in ionic interfaces from first-principles calculations. The Journal of Physical Chemistry C 2014, 118, 30139-30144.
32. Mouyane, M.; Itaalit, B.; Bernard, J.; Houivet, D.; Noudem, J.G. Flash combustion synthesis of electron doped-CaMnO3 thermoelectric oxides. Powder technology 2014, 264, 71-77.
33. Torres, S.d.O.; Thomazini, D.; Balthazar, G.P.; Gelfuso, M.V. Microstructural influence on thermoelectric properties of CaMnO3 ceramics. Materials Research 2020, 23, e20200169.
34. Kanas, N.; Williamson, B.A.; Steinbach, F.; Hinterding, R.; Einarsrud, M.-A.; Selbach, S.M.; Feldhoff, A.; Wiik, K. Tuning the thermoelectric performance of CaMnO3-based ceramics by controlled exsolution and microstructuring. ACS Applied Energy Materials 2022, 5, 12396-12407.
35. Singh, S.P.; Kanas, N.; Desissa, T.D.; Einarsrud, M.-A.; Norby, T.; Wiik, K. Thermoelectric properties of non-stoichiometric CaMnO3-δ composites formed by redox-activated exsolution. Journal of the European Ceramic Society 2020, 40, 1344-1351.
36. Martin, J. Protocols for the high temperature measurement of the Seebeck coefficient in thermoelectric materials. Measurement Science and Technology 2013, 24, 085601.
37. Snyder, G.J.; Snyder, A.H.; Wood, M.; Gurunathan, R.; Snyder, B.H.; Niu, C. Weighted mobility. Advanced Materials 2020, 32, 2001537.
38. Katase, T.; He, X.; Tadano, T.; Tomczak, J.M.; Onozato, T.; Ide, K.; Feng, B.; Tohei, T.; Hiramatsu, H.; Ohta, H. Breaking of Thermopower–Conductivity Trade-Off in LaTiO3 Film around Mott Insulator to Metal Transition. Advanced Science 2021, 8, 2102097.
39. Hong, W.T.; Gadre, M.; Lee, Y.-L.; Biegalski, M.D.; Christen, H.M.; Morgan, D.; Shao-Horn, Y. Tuning the spin state in LaCoO3 thin films for enhanced high-temperature oxygen electrocatalysis. The journal of physical chemistry letters 2013, 4, 2493-2499.
40. Mitterdorfer, A.; Gauckler, L. La2Zr2O7 formation and oxygen reduction kinetics of the La0. 85Sr0. 15MnyO3, O2 (g)| YSZ system. Solid State Ionics 1998, 111, 185-218.
41. Lan, Z.; Vegge, T.; Castelli, I.E. Exploring the electronic properties and oxygen vacancy formation in SrTiO3 under strain. Computational Materials Science 2024, 231, 112623.
42. Xi, J.; Xu, H.; Zhang, Y.; Weber, W.J. Strain effects on oxygen vacancy energetics in KTaO 3. Physical Chemistry Chemical Physics 2017, 19, 6264-6273.
43. Aidhy, D.S.; Rawat, K. Coupling between interfacial strain and oxygen vacancies at complex-oxides interfaces. Journal of Applied Physics 2021, 129.
44. Lee, K.H.; Kim, S.i.; Lim, J.C.; Cho, J.Y.; Yang, H.; Kim, H.S. Approach to determine the density-of-states effective mass with carrier concentration-dependent Seebeck coefficient. Advanced Functional Materials 2022, 32, 2203852.
45. Bhansali, S.; Khunsin, W.; Chatterjee, A.; Santiso, J.; Abad, B.; Martín-González, M.; Jakob, G.; Torres, C.S.; Chávez-Angel, E. Enhanced thermoelectric properties of lightly Nb doped SrTiO 3 thin films. Nanoscale advances 2019, 1, 3647-3653.
46. Li, G.; Liu, S.; Piao, Y.; Jia, B.; Yuan, Y.; Wang, Q. Joint improvement of conductivity and Seebeck coefficient in the ZnO: Al thermoelectric films by tuning the diffusion of Au layer. Materials & Design 2018, 154, 41-50.
47. Schmidt, V.; Mensch, P.F.; Karg, S.F.; Gotsmann, B.; Das Kanungo, P.; Schmid, H.; Riel, H. Using the Seebeck coefficient to determine charge carrier concentration, mobility, and relaxation time in InAs nanowires. Applied Physics Letters 2014, 104.
48. Roguai, S.; Djelloul, A. Sn doping effects on the structural, microstructural, Seebeck coefficient, and photocatalytic properties of ZnO thin films. Solid State Communications 2022, 350, 114740.
49. Wang, S.; Xiao, Y.; Ren, D.; Su, L.; Qiu, Y.; Zhao, L.-D. Enhancing thermoelectric performance of BiSbSe3 through improving carrier mobility via percolating carrier transports. Journal of Alloys and Compounds 2020, 836, 155473.

 doi:10.20944/preprints202511.1059.v1

50. Movaghar, B.; Jones, L.O.; Ratner, M.A.; Schatz, G.C.; Kohlstedt, K.L. Are transport models able to predict charge carrier mobilities in organic semiconductors? The Journal of Physical Chemistry C 2019, 123, 29499-29512.
51. Chen, A.; Zhu, K.; Zhong, H.; Shao, Q.; Ge, G. A new investigation of oxygen flow influence on ITO thin films by magnetron sputtering. Solar energy materials and solar cells 2014, 120, 157-162.
52. Werner, F. Hall measurements on low-mobility thin films. Journal of Applied Physics 2017, 122.
53. El Loubani, M.; Yang, G.; Kouzehkanan, S.M.T.; Oh, T.-S.; Balijepalli, S.K.; Lee, D. Influence of redox engineering on the trade-off relationship between thermopower and electrical conductivity in lanthanum titanium-based transition metal oxides. Materials Advances 2024, 5, 9007-9017.